# Complex dynamics in double-diffusive convection

**Esteban Meca*, Isabel Mercader, Oriol Batiste, Laureano Ramírez-Piscina**

Departament de Física Aplicada, Universitat Politècnica de Catalunya, Barcelona, Spain
e-mail: esteban@fa.upc.es - Web page: http://www-fa.upc.es/

**ABSTRACT**

Double-diffusive fluxes occur when convection is driven by thermal and concentration gradients, and the temperature and concentration diffusivities take different values. This phenomenon has relevance for numerous applications [1]. From a theoretical point of view very interesting behavior has been found in cavities with imposed vertical gradients, including chaos [2]. The case of horizontal gradients naturally arises in applications such as crystal growth. In this configuration, quiescent (conductive) solutions do exist when thermal and solutal buoyancy forces exactly compensate each other. This has allowed for theoretical analysis by studying the stability of the conductive solution [3, 4, 5, 6]. In this work we numerically study this later case for a small Prandtl number binary mixture, including only the Soret effect. On one hand we have calculated the branches of steady states and their stability, locating the bifurcation points, and on the other hand we have found non steady solutions by performing temporal integration of the evolution equations.

We have considered a binary mixture in a 2-D rectangular cavity of aspect ratio $\Gamma = d/h = 2$, where $d$ is the length and $h$ is the height of the cavity. A difference of temperature $\Delta T$ is maintained between both vertical boundaries. Dimensionless equations in Boussinesq approximation explicitly read

$$\begin{aligned} \nabla \cdot \mathbf{u} &= 0, \\ \partial_t \mathbf{u} + (\mathbf{u}\cdot\nabla)\mathbf{u} &= -\nabla P + \sigma\nabla^2\mathbf{u} + \sigma Ra[(1+S)(-0.5 + x/\Gamma + \theta) + S\eta]\hat{\mathbf{z}}, \\ \partial_t \theta + (\mathbf{u}\cdot\nabla)\theta &= -u/\Gamma + \nabla^2\theta, \\ \partial_t \eta + (\mathbf{u}\cdot\nabla)\eta &= \tau\nabla^2\eta - \nabla^2\theta, \end{aligned} \tag{1}$$

where $\mathbf{u} \equiv (u, w)$ is the dimensionless velocity field in $(x, z)$ coordinates, $P$ is the pressure over the density, and $\theta$ denotes the departure of the temperature from a linear horizontal profile, in units of $\Delta T$. Lengths and times are scaled with $h$ and $t_\kappa = h^2/\kappa$, respectively, being $\kappa$ the thermal diffusivity. The dimensionless parameters are the Prandtl number $\sigma = \nu/\kappa$, the Rayleigh number $Ra = \alpha g h^3 \Delta T/\nu\kappa$ and the Lewis number $\tau = D/\kappa$, where $\nu$ denotes the kinematic viscosity, $g$ the gravity level, $\alpha$ the thermal expansion coefficient, and $D$ is the mass diffusivity. The separation ratio $S = C_0(1 - C_0)\frac{\beta}{\alpha}S_T$ will be taken $S = -1$. Here, $S_T$ is the Soret coefficient, $C_0$ is the concentration of the heavier component in the homogeneous mixture, and $\beta$ is the mass expansion coefficient ($\beta > 0$ for the heavier component). The variable $\eta = C - \theta$ represents a dimensionless chemical potential, being $C$ the deviation of the concentration of the heavier component relative to the linear horizontal profile which equilibrates that of the temperature in the expression of the mass flux. The gradient of $\eta$ represents the dimensionless mass flux.

The boundaries are taken to be no-slip and with no mass flux. Right and left hand sides are maintained at constant temperatures and at the horizontal plates a linear profile of temperature between the two prescribed temperatures is imposed. Thus, boundary conditions are written as

$$\mathbf{u} = \theta = \mathbf{n}\cdot\nabla\eta = 0, \quad \text{at } \delta\Omega. \tag{2}$$

These boundary conditions prevent the transformation that takes the Soret equations into those used in Refs.[3, 4, 5, 6]. Equations (1) together with boundary conditions (2), are invariant under a rotation of $\pi$ around the point $(\Gamma/2, 1/2)$.

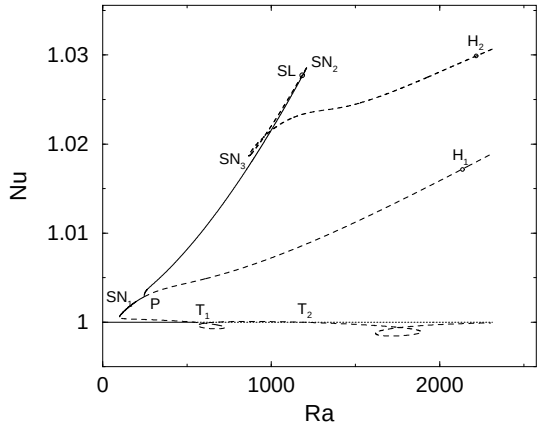


Figure 1: Stationary solutions diagram

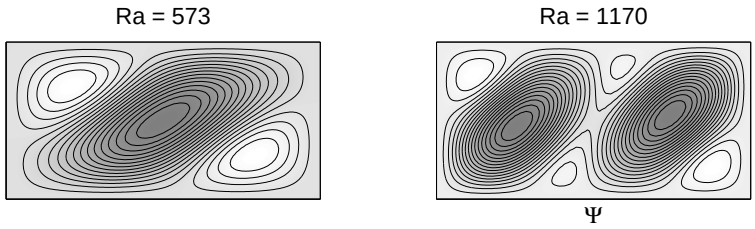


Figure 2: Stream lines of the steady solutions of $Ra = 573$ and $Ra = 1170$.

We have solved equations (1) and boundary conditions (2) using a second order time-splitting algorithm, proposed in [7], applied to a pseudo-spectral Chebyshev method. To calculate steady solutions we have adapted a pseudoespectral first-order time-stepping formulation to carry out Newton's method, as described in Refs [8, 9, 10]. In the preconditioned version of the Newton's iteration, the corresponding linear system is solved by an iterative technique using a GMRES package (CERFACS, free distribution). The linear stability analysis of the steady states is conducted by computing the leading eigenvalues of the Jacobian by means of the Arnoldi's method, using routines from the ARPACK package.

For numerical calculations the chosen parameters have been Prandtl number $\sigma = 0.00715$ and Lewis number $\tau = 0.03$. Analysis of the steady solutions provides the scenario shown in Fig. 1. For small $Ra$ the conductive solution (allowed by the choice $S = -1$) is stable, but loses stability at $Ra = 541.9$ through a transcritical bifurcation ($T_1$) maintaining symmetry. The bifurcating solutions are characterized by a central main roll accompanied by secondary ones in opposed corners. The supercritical branch is stable only until $Ra = 542.4$, where a small non-symmetric branch connect it to the conductive solutions through pitchfork bifurcations, as in Ref. [5]. The unstable symmetric branch undergoes a couple of saddle node bifurcations until it crosses through a transcritical bifurcation the conductive branch at $Ra = 1164$ ($T_2$). In this process the number of rolls increases. This is shown if Fig. 2, where stream lines are shown for the (unstable) steady solutions corresponding to $Ra = 573$ and $Ra = 1170$. All this branch is characterized by very small fluxes, and hence by very small departures of the temperature and concentration profiles from that corresponding to the (constant gradients) conductive solution.

The subcritical branch gains stability in a saddle node bifurcation at $Ra = 99$ ($SN_1$), and loses it again at $Ra = 245$ in a Pitchfork bifurcation ($P$) where a stable non-symmetric branch appears. A comparison

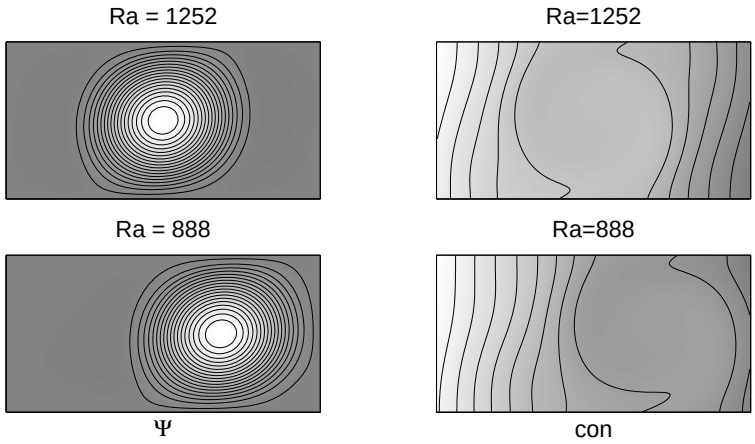


Figure 3: Stream lines and concentration levels of the steady solutions of the symmetric branch ($Ra = 1252$) and the non symmetric branch ($Ra = 888$).

between both branches is shown in Fig. 3. They are both characterized by a main roll, centered in the case of the symmetric solution (Fig. 3.a) and confined to one side in the broken-symmetry solution (Fig. 3.b). Concentration fields are roughly homogeneous inside rolls, displacing concentration gradients to the lateral boundaries.

Following these two branches, one finds the following: On the one hand the steady asymmetrical solution undergoes two successive saddle-node bifurcations at $Ra = 1209$ ($SN_2$) (losing stability) and $Ra = 865.6$ ($SN_3$). At $Ra = 2218$ we found a Hopf bifurcation ($H_2$). Therefore from $Ra = 1209$ on there is a region in which no steady stable solution exist. On the other hand the steady symmetrical solution suffers a Hopf bifurcation at $Ra = 2137$ ($H_1$) that mantains the symmetry. The (still unstable) bifurcating orbit has been then calculated by using temporal evolution forcing the symmetry. At $Ra = 2253$ this solution gains stability in a Pitchfork bifurcation. The new non-symmetric orbit is unstable and we could not follow it. Nevertheless it is presumably connected to the former asymmetric branch at the Hopf bifurcation of $Ra = 2218$, since that agrees with our proposed scenario.

Beyond $Ra = 1209$, from temporal integration of the evolution equations we have obtained a branch of asymmetric periodic solutions. When the Rayleigh number decreases, the period of this orbit becomes logarithmically singular and we have identified a global saddle-loop bifurcation [11] at $Ra = 1184$ ($SL$), when the orbit connects with the unstable branch of the saddle-node of $Ra = 1209$. The logarithmic fit of these periods gave the same value of the unstable eigenvalue of the saddle stationary point than that obtained by the steady state stability calculation. Near the global bifurcation the time evolution of the velocity of a representative point is shown in Fig. 4 (left).The value for the steady asymmetric unstable solution is also represented. We see how the solution spends a long time near the steady solution.

This asymmetric periodic orbit is the only observed solution until $Ra = 2253$, where the symmetric periodic solution mentioned above becomes stable. Then both solutions coexist until $Ra = 2257.5$, where the asymmetric orbit disappears.

The Hopf bifurcation that undergoes the symmetric steady state at $Ra = 2137$ is reflected in the shape of the asymmetric orbit and when we increase further $Ra$, the period of the orbit diverges as $Ra^{-1/2}$. Also, the system follows a period doubling cascade. The attractor is represented if Fig. 4 (right) for $Ra = 2255$. The attractor disappears at $Ra = 2258$ after reaching an infinite period and infinite length

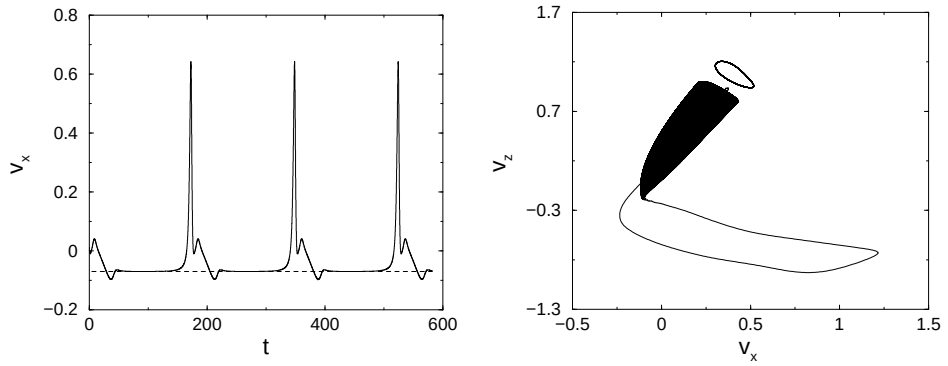


Figure 4: Asymmetric orbit. Left: time series near $Ra = 1184$, with the value of the saddle stationary solution marked. Right: attractor for $Ra = 2255$. The stable symmetric orbit is also represented

limit. The process through which the attractor disappears is not completely clear. The law of growth of the period suggests that there is a connection with a saddle-node. This, together with the divergence in the length of the orbit, is consistent with a 'blue sky catastrophe' scenario [12].

## REFERENCES


[1] J.S. Turner, *Multicomponent Convection,* Ann. Rev. Fluid Mech. **17**, 11-44, 1985, and references therein.

[2] E. Knobloch, D.R. Moore, J. Toomre and N.O. Weiss, *Transition to chaos in two-dimensional double-diffusive convection,* J. Fluid Mech. **166**, 409-448, 1986.

[3] K. Ghorayeb and A. Motjabi, *Doubly diffusive convection in a vertical rectangular cavity*, Phys. Fluids **9**, 2339-2348 (1997).

[4] S. Xin, P. Le Quéré and L. Tuckerman, *Bifurcation analysis of doubly-diffusive convection with opposing horizontal thermal and solutal gradients*, Phys. Fluids **10**, 850-858 (1997).

[5] G. Bardan, A. Bergeon, E. Knobloch and A. Motjabi, *Nonlinear doubly diffusive convection in vertical enclosures*, Physica D **138**, 91-113, 2000.

[6] A. Bergeon and E. Knobloch, *Natural doubly diffusive convection in three-dimensional enclosures*, Phys. Fluids **14**, 3233-3250, 2002.

[7] S. Hugues and A. Randiamampianina, *An improved projection scheme applied to pseudospectral method for the incompressible Navier-Stokes equations*, Int. J. Numer. Methods Fluids **28**, 501 (1998).

[8] C.K. Mamum and L.S. Tuckerman, *Asymmetry and Hopf bifurcation in spherical Couette flow*, Phys. Fluids **7**, 80 (1995).

[9] A. Bergeon, D. Henry, H. Benhadid and L.S. Tuckerman, *Marangoni convection in binary mixtures with Soret effect*, J. Fluid Mech. **375**, 143 (1998).

[10] S. Xin, P. Le Quéré, *Linear stability analyses of natural convection in a differentially heated square cavity with conducting horizontal walls*, Phys. Fluids **13** (9), 2529 (2001).

[11] S. Schecter, *The saddle-node separatrix-loop bifurcation*, SIAM J. Math. Anal. **18** (4), 1142 (1987).

[12] Y.A. Kuznetsov, *Elements of Applied Bifurcation Theory*, Applied Mathematical Sciences Vol 112, Springer-Verlag (1985).